

Lawrence Berkeley National Laboratory

LBL Publications

Title

Effects of O₂ plasma and UV-O₃ assisted surface activation on high sensitivity metal oxide functionalized multiwalled carbon nanotube CH₄ sensors

Permalink

<https://escholarship.org/uc/item/20h1b172>

Journal

Journal of Vacuum Science & Technology A Vacuum Surfaces and Films, 35(6)

ISSN

0734-2101

Authors

Humayun, Tanim
Sainato, Michela
Divan, Ralu
[et al.](#)

Publication Date

2017-11-01

DOI

10.1116/1.4993579

Copyright Information

This work is made available under the terms of a Creative Commons Attribution-ShareAlike License, available at <https://creativecommons.org/licenses/by-sa/4.0/>

Peer reviewed

Effects of O₂ plasma and UV-O₃ assisted surface activation on high sensitivity metal oxide functionalized multiwalled carbon nanotube CH₄ sensors

Md Tanim Humayun, Michela Sainato, Ralu Divan, Richard A. Rosenberg, Alvaro Sahagun, Lara Gundel, Paul A. Solomon, and Igor Paprotny

Citation: *Journal of Vacuum Science & Technology A: Vacuum, Surfaces, and Films* **35**, 061402 (2017);

View online: <https://doi.org/10.1116/1.4993579>

View Table of Contents: <http://avs.scitation.org/toc/jva/35/6>

Published by the [American Vacuum Society](#)

Articles you may be interested in

[Ultradeep electron cyclotron resonance plasma etching of GaN](#)

Journal of Vacuum Science & Technology A: Vacuum, Surfaces, and Films **35**, 061303 (2017);
10.1116/1.4994829

[Self-catalyst assisted and catalyst-free epitaxial growth of InAs on Ge \(111\): Role of substrate surface and evolution of polytypism](#)

Journal of Vacuum Science & Technology A: Vacuum, Surfaces, and Films **35**, 061501 (2017);
10.1116/1.4996104

[Low-temperature and scalable CVD route to WS₂ monolayers on SiO₂/Si substrates](#)

Journal of Vacuum Science & Technology A: Vacuum, Surfaces, and Films **35**, 061502 (2017);
10.1116/1.4996550

[Oxidation behavior of intermetallic Al-Cr and Al-Cr-Fe macroparticles](#)

Journal of Vacuum Science & Technology A: Vacuum, Surfaces, and Films **35**, 061601 (2017);
10.1116/1.4986928

[Interaction of ammonia and hydrogen with tungsten at elevated temperature studied by gas flow through a capillary](#)

Journal of Vacuum Science & Technology A: Vacuum, Surfaces, and Films **35**, 061602 (2017);
10.1116/1.4995373

[Ag⁺ reduction and silver nanoparticle synthesis at the plasma-liquid interface by an RF driven atmospheric pressure plasma jet: Mechanisms and the effect of surfactant](#)

Journal of Vacuum Science & Technology A: Vacuum, Surfaces, and Films **35**, 061302 (2017);
10.1116/1.4995374




Instruments for Advanced Science

Contact Hiden Analytical for further details:
W www.HidenAnalytical.com
E info@hiden.co.uk
CLICK TO VIEW our product catalogue




Gas Analysis

- dynamic measurement of reaction gas streams
- catalysis and thermal analysis
- molecular beam studies
- dissolved species probes
- fermentation, environmental and ecological studies




Surface Science

- UHV TPD
- SIMS
- end point detection in ion beam etch
- elemental imaging - surface mapping



Plasma Diagnostics

- plasma source characterization
- etch and deposition process reaction
- kinetic studies
- analysis of neutral and radical species



Vacuum Analysis

- partial pressure measurement and control of process gases
- reactive sputter process control
- vacuum diagnostics
- vacuum coating process monitoring

Effects of O₂ plasma and UV-O₃ assisted surface activation on high sensitivity metal oxide functionalized multiwalled carbon nanotube CH₄ sensors

Md Tanim Humayun and Michela Sainato

Department of Electrical and Computer Engineering, University of Illinois at Chicago, Chicago, Illinois 60607

Ralu Divan

Center for Nanoscale Materials, Argonne National Laboratory, Argonne, Illinois 60439

Richard A. Rosenberg

Advanced Photon Source, Argonne National Laboratory, Argonne, Illinois 60439

Alvaro Sahagun

Department of Electrical and Computer Engineering, University of Illinois at Chicago, Chicago, Illinois 60607

Lara Gundel

Lawrence Berkeley National Laboratory, Berkeley, California 94720

Paul A. Solomon

U.S. Environmental Protection Agency, Las Vegas, Nevada 89199

Igor Paprotny^{a)}

Department of Electrical and Computer Engineering, University of Illinois at Chicago, Chicago, Illinois 60607

(Received 1 October 2016; accepted 26 June 2017; published 28 July 2017)

The authors present a comparative analysis of ultraviolet-O₃ (UVO) and O₂ plasma-based surface activation processes of multiwalled carbon nanotubes (MWCNTs), enabling highly effective functionalization with metal oxide nanocrystals (MONCs). Experimental results from transmission electron microscopy, scanning electron microscopy, x-ray photoelectron spectroscopy, and Raman spectroscopy show that by forming COOH (carboxyl), C-OH (hydroxyl), and C=O (carbonyl) groups on the MWCNT surface that act as active nucleation sites, O₂ plasma and UVO-based dry pretreatment techniques greatly enhance the affinity between the MWCNT surface and the functionalizing MONCs. MONCs, such as ZnO and SnO₂, deposited by the atomic layer deposition technique, were implemented as the functionalizing material following UVO and O₂ plasma activation of MWCNTs. A comparative study on the relative resistance changes of O₂ plasma and UVO activated MWCNT functionalized with MONC in the presence of 10 ppm methane (CH₄) in air is presented as well. © 2017 American Vacuum Society. [<http://dx.doi.org/10.1116/1.4993579>]

I. INTRODUCTION

Methane (CH₄) gas has a 100 year global warming impact factor of 24–36 compared to CO₂.¹ With the emergence of the U.S. as the world's leading producer of natural gas, it is important to enable widespread monitoring of CH₄ emission from natural gas infrastructures. Metal oxide chemoresistive sensors are widely used to sense CH₄.^{2–4} Continuous heating is necessary for these sensors to initiate the surface chemisorption of O₂, a prerequisite to detect CH₄, often requiring 100 s of milliwatts of power.^{2–5} Carbon nanotube (CNT)-based chemoresistor sensors have demonstrated ppm levels of gas sensing at room temperature, with a power consumption of only a few milliwatts.⁵ This is a direct outcome of CNT's high surface-to-volume ratio and outstanding modulation of electrical conductance during interaction with gas species. However, functionalizing particles (ranging

from metal,⁵ metal oxides,⁶ and polymer coating⁷ to biomolecules⁸) must be deposited uniformly on the surface of pristine carbon nanotubes in order to enable effective and reversible electrical modulation in the presence of target gas species. Unfortunately, in general, the surface of CNTs shows poor affinity with the functionalizing materials.^{9–13} Consequently, before applying the functionalization materials, *activation* of the inert graphitic surface of the CNTs is necessary.^{9–11}

We present here a comparative analysis of novel UV-O₃ (UVO) and O₂ plasma-based surface activation processes, which enables highly effective functionalization of multiwalled carbon nanotubes (MWCNTs) with metal oxide nanocrystals (MONCs). O₂ plasma and UVO-based dry surface activation techniques have not been applied in CNT-based CH₄ chemoresistor sensors before.^{5,14,15} Weak affinity among the CNT surface and the functionalizing nanoparticles, resulting from the absence of surface activation, may greatly affect the sensor's reversible response to low ppm

^{a)}Electronic mail: paprotny@uic.edu

methane concentrations. Experimental results from transmission electron microscopy (TEM), scanning electron microscopy (SEM), x-ray photoelectron spectroscopy (XPS), and Raman spectroscopy show that by forming carboxyl (COOH), hydroxyl (C-OH), and carbonyl (C=O) groups on the MWCNT surface, which act as active nucleation sites, O₂ plasma and UVO-based dry activation techniques greatly enhance the affinity between the MWCNT surface and the functionalizing MONCs. We have implemented MONCs such as ZnO and SnO₂ as the functionalizing material following UVO and O₂ plasma activation of MWCNTs. MONCs were deposited by the atomic layer deposition (ALD) technique.^{16–18} These metal oxides are less expensive than previously reported functionalizing materials (e.g., Pd) used in CNT-based CH₄ sensors.^{5,6} Electron transport is energetically favorable in the ZnO-MWCNT or SnO₂-MWCNT junctions, whereas Pd forms a significant Schottky barrier with bare CNTs.^{5,6,19,20} A comparative study on the relative resistance changes of O₂ plasma and UVO activated MONC functionalized MWCNT chemoresistive sensors, in the presence of 10 ppm CH₄ in air, is presented. After CH₄ exposure, the sensors were recovered to baseline resistance by N₂ purging. An analysis of the effect of relative humidity (RH) on the sensor response is also presented, showing superior performance to other previously reported CNT CH₄ sensors.

Traditionally, the surface of bare CNTs is activated by exposing them to high temperature vapors¹⁰ and/or using wet chemistry.¹¹ High temperature or air exposure may actually destroy or excessively damage the CNTs.¹⁰ Acid treatments used in wet chemistry can considerably reduce the mechanical and electric performance of the tubes by introducing large numbers of defects.²¹ Wet chemistry also involves additional steps, such as dissolution, sonication, mixing, and drying, which often causes undesirable agglomeration of treated CNTs.¹⁰

To increase the efficiency of CNT functionalization, two alternative dry activation processes have been proposed: (1) gas plasma^{9–11} and (2) UVO treatment.²²

Due to the interaction of surface C atoms with active O atoms during O₂ plasma or UVO activation and subsequent exposure to the atmosphere, chemical groups such as COOH, C=O, C-OH, and ether (C-O-C) are formed on the MWCNT surface.^{11–13,23,24} These groups act as active sites for the nucleation of MONCs.^{11–13,22} Both the O₂ plasma and UVO exposure have no effect on the aspect ratio (i.e., length to diameter ratio) of the MWCNTs.²¹

II. EXPERIMENT

A. Sensor fabrication

We fabricated surface activated MONC (ZnO or SnO₂) functionalized MWCNT chemoresistive CH₄ sensors using the following fabrication steps: (1) lift-off based photolithography, (2) O₂ plasma or UVO based surface activation, and (3) ALD based functionalization. The sensor concept is illustrated in Fig. 1(a). Figure 1(b) shows an SEM image of the

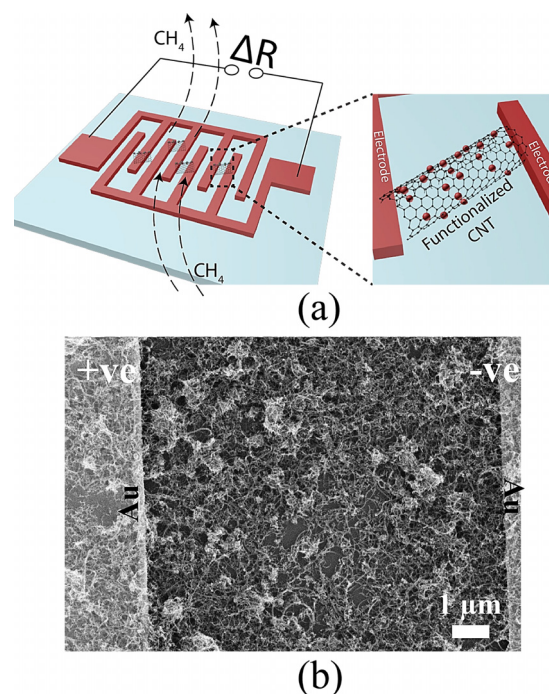


Fig. 1. (Color online) (a) Concept of MONC-MWCNT CH₄ chemoresistive sensors. The sensors act as resistors that change resistance when exposed to CH₄. (b) SEM image of ZnO functionalized MWCNTs confined between two Au electrodes.

sensor where functionalized MWCNTs can be seen deposited between a pair of Au electrodes.

Interdigitated Au electrodes were fabricated by photolithography. Details on the fabrication process can be found elsewhere.²⁵

MWCNT (98% pure) with an average diameter of 12 nm, an average length of 10 μm, and a specific surface area of 220 m²/g was purchased from Sigma Aldrich. Using a microsyringe, an aliquot of 50 μl from a 1 g/50 ml solution of MWCNT-ethanol was deposited on an active area of 1 mm² on the fabricated Au electrodes. It was followed by baking the devices at 75 °C to remove ethanol and improve adhesion.

The deposited MWCNTs were O₂ plasma activated in a reactive ion etching chamber (March plasma CS-1701). The base pressure of the plasma chamber was almost 40 mTorr. O₂ was introduced at a flow rate of 20 sccm, while the pressure was maintained at 160 mTorr during the process. O₂ plasma was generated by applying a radio frequency of 13.56 MHz with a power of 100 watts. The duration of the plasma treatment was 5 min. A UVO cleaner (Nanonex Ultra 100) was used for the UVO treatment of the MWCNT surface where a 185 nm UV was radiated to atmosphere for generating O₃ and activating the MWCNT surface. The process duration was 20 min.

Using diethylzinc [(C₂H₅)₂Zn] as a precursor, ALD of ZnO on the surface activated MWCNTs was performed using an Arradiance Gemstar ALD tool (details can be found in Ref. 25).

ALD was also used to deposit SnO₂ nanocrystals (NCs) onto the surface activated MWCNTs. The growth was carried out using an Ultratech Savannah S200 with

tetrakis(dimethylamino)tin(IV) as a precursor (details can be found in Ref. 26).

B. TEM sample preparation and imaging

Holey carbon films on Cu grids were used to prepare the TEM sample. Using a microsyringe, an aliquot of 50 μl from a 1 mg/50 μl solution of MWCNT-ethanol solution was deposited on the TEM grid. It was followed by baking the devices at 75 $^{\circ}\text{C}$ to remove ethanol and improve adhesion. MWCNTs were surface activated in a similar manner as described in Sec. II A (5 min O₂ plasma or 20 min UVO).

ALD of ZnO or SnO₂ was performed following a similar approach described in Subsec. II A.

A JEOL 2100F TEM operating at 200 kV was used to characterize the atomic scale morphology and crystal quality of the MONCs deposited on MWCNT surfaces.

C. XPS sample preparation

Au of 20 nm was deposited on a clean Si wafer using electron beam evaporation. Using a microsyringe, an aliquot of relatively higher density solution (1 mg/1 μl) of MWCNT-ethanol was deposited on the Au-coated Si wafers. It was followed by baking the devices at 75 $^{\circ}\text{C}$ to remove ethanol and improve adhesion. MWCNTs were surface activated in a similar manner as described in Sec. II A (5 min O₂ plasma or 20 min UVO).

D. Test setup and approach

Sensors were exposed to a 10 ppm mixture of CH₄ in synthetic air (20.81% of O₂ and 79.19% of N₂; prepared by Praxair Inc.). The flow rate was maintained at 0.94 l/min with a residence time of 4.5 min inside the plastic test chamber (details elsewhere²⁵). After the CH₄ exposure, the sensors were flushed with N₂ (the same flow rate as CH₄, 0.94 l/min). The electrical signal obtained from the sensors was recorded using a custom interface circuit connected to a computer. A onset HOBO U12 series data logger

temperature and RH sensor was used to continuously monitor and record the RH and temperature inside the plastic test chamber during the test.

III. RESULTS AND DISCUSSION

A. Sample characterization

High resolution XPS ($h\nu = 650\text{ eV}$) was carried out using beamline 4-ID-C at the Advanced Photon Source, Argonne National Laboratory. MWCNTs were deposited on gold-covered silicon substrates and subsequently activated by O₂ plasma or UVO. Binding energies were calibrated to the Au 4f binding energy of 84.0 eV. Quantification was performed using XPS data analysis software CASAXPS. Figure 2 shows the C 1s and O 1s peaks originating from pristine [(a) and (d)] and 5 min O₂ plasma activated [(b) and (e)] and 20 min UVO activated MWCNT [(c) and (f)]. The assignments of the C 1s and O 1s components were based on reported spectra containing specific oxygen functional groups.^{24,27–29} The measured spectra were fitted to a function having 70% Gaussian and 30% Lorentzian character, after performing a Shirley background correction. The C1 component centered at 284.3 eV represents the sp^2 graphitic component. The components at 285.4, 286.5, 287.7, and 289.1 eV (C2 up to C5) were assigned to C atoms forming C-OH, C-O-C, C=O, and COOH functional groups, respectively;^{24,27–29} the components at 531.1 eV (O1), 532.2 eV (O2), 533.5 eV (O3), and 534.7 eV (O4) were assigned to O atoms forming C=O, C-OH, C-O-C, and H₂O, respectively.^{24,27–29}

The normalized peak areas (NPA) of various components of C 1s and O 1s spectra were calculated with respect to the area of their respective C1 component (sp^2) (Table I). Comparison among the NPA of C5 (COOH group) in several samples suggests that COOH is the primary chemical group created by the surface activation process. The NPA of C-OH components (C2 and O2) are significantly larger in the surface activated sample compared to the pristine sample, suggesting the strong presence of C-OH in the surface activated

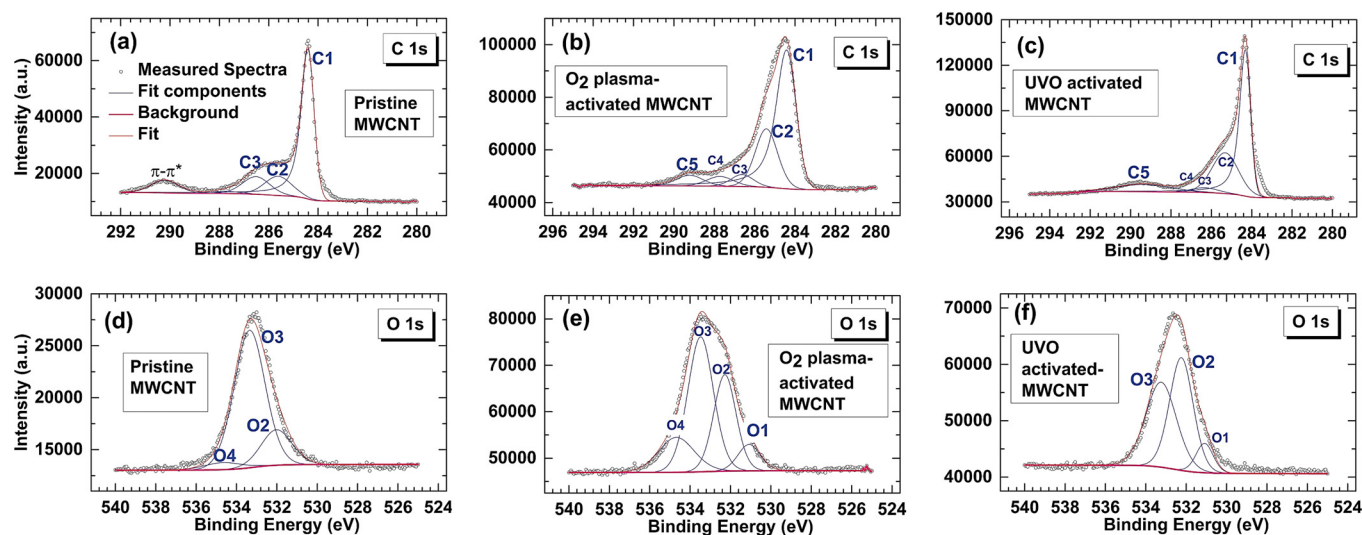


Fig. 2. (Color online) (a)–(c) C 1s XPS peaks: (a) pristine MWCNTs, (b) 5 min O₂ plasma activated MWCNTs, and (c) 20 min UVO activated MWCNTs. (d)–(f) O 1s XPS peaks: (d) pristine MWCNTs, (e) 5 min O₂ plasma activated MWCNTs, and (f) 20 min UVO activated MWCNTs.

TABLE I. Comparison between NPA (with respect to C1) of C 1s (C2 to C5) and O 1s (O1 to O3) peak components in pristine, plasma activated, and UVO activated MWCNT samples.

Peak component	Location (eV)	Functional group	NPA		
			Pristine MWCNT	Plasma activated MWCNT	UVO activated MWCNT
C2	285.4	C-OH	0.29	0.50	0.73
C3	286.5	C-O-C	0.26	0.10	0.08
C4	287.7	C=O	0.03	0.10	0.02
C5	289.1	COOH	Not present	0.11	0.26
O1	531.1	C=O	0.02	0.13	0.09
O2	532.2	C-OH	0.20	0.47	0.48
O3	533.5	C-O-C	0.77	0.76	0.47

MWCNT as well. The NPA of C4 and O1, representing the C=O group, were found to be highest in the 5 min plasma activated MWCNT but insignificant in pristine and 20 min UVO activated MWCNT. On the other hand, the NPA of the C3 and O3, representing the C-O-C functional group, were found to be highest in the pristine MWCNT (Table I).

It is well known that active π bonds in C=C are dissociated during plasma/UVO activation and -C. free radicals are produced.^{11,23,24} Subsequently, -C. free radicals are oxidized by active O atoms present in the O₂ plasma and UVO, resulting in C-O and C=O bonds.^{23,24} After prolonged interaction with plasma/UVO, C=O is further oxidized and O-C=O is formed.^{23,24} Due to atmospheric exposure, C-O and O-C=O stabilize by reacting with ambient H₂O and generate C-OH and COOH, respectively.²³ This is the probable cause of the strong presence of COH and COOH groups in our plasma/UVO activated MWCNTs. Surface C atoms of pristine MWCNT react with atmospheric H₂O to create C-O, a probable cause of the presence of the C-O-C group in pristine MWCNT.²⁴

In summary, the XPS results corroborate that the surface activation process produces the COOH functional group along with C-OH and C=O. In later steps, these groups help in nucleating the functionalizing MONCs on the surface of the MWCNTs.

The TEM micrographs show that MONCs are not visible on the surface of the nonactivated but ALD processed MWCNTs [Fig. 3(a)]. Uniform deposition of ZnO-MONCs was found on the surface of the activated MWCNTs [Fig. 3(b)]. The clearly visible lattice fringes in the higher resolution TEM (HRTEM) image in Fig. 3(d) illustrate the wurtzite structure of the ZnO MONC and its good crystalline quality. The interplanar spacings of 2.8, 2.68, and 2.48 Å correspond to the $\langle 100 \rangle$, $\langle 002 \rangle$, and $\langle 101 \rangle$ planes of ZnO, respectively.³⁰ The HRTEM image in Fig. 3(c) shows the atomic scale morphology of rutile SnO₂ MONCs deposited on the MWCNT surface. The interplanar spacings of 2.6 and 3.3 Å correspond to $\langle 101 \rangle$ and $\langle 110 \rangle$ planes of SnO₂, respectively.⁶ TEM results validate the hypothesis that surface activation of the MWCNTs is essential for effective functionalization, i.e., nucleation and stronger binding of the MONCs to the surfaces of the MWCNTs.

Room temperature Raman spectroscopy was performed using a Renishaw Invia micro-Raman system with a 514 nm

laser. Three types of ZnO ALD functionalized MWCNT samples were used in the Raman characterization: (1) O₂ plasma activated, (2) UVO activated, and (3) nonactivated, i.e., untreated. Raman spectra, illustrated in Fig. 4, reveal that after the surface activation and ALD functionalization, the D, G, and G' band peaks of the MWCNTs are preserved, while additional Raman peaks originating from the ZnO NCs appeared. The characteristic Raman peaks of ZnO NCs represented by *m*, *n*, *o*, and *p* were observed only on the O₂ plasma activated samples (1), *n*, *o*, and *p*, were observed on the UVO activated samples (2), while none of these peaks were visible on the untreated MWCNT samples (3), consistent with the hypothesis that the ZnO NC functionalization is enhanced in surface-activated MWCNTs. The peaks described in Fig. 4(b)—200.6 cm⁻¹ (*m*), 324.25 cm⁻¹ (*n*), 430.84 cm⁻¹ (*o*), 569.87 cm⁻¹ (*p*)—correspond to $2E_2^{\text{low}}$, $E_2^{\text{high}} - E_2^{\text{low}}$, E_2^{high} , and $A_1(\text{LO})$ modes of ZnO,^{31,32} respectively, suggesting that surface activated samples have ZnO NCs with high crystalline quality. In addition, the characteristic ZnO Raman peaks are sharper in O₂ plasma activated MWCNTs than in UVO activated MWCNTs. The full width at half maximum of the A₁(LO) peak was found to be 50.5 and 62.29 cm⁻¹ for O₂ plasma activated and UVO activated samples, respectively, also suggesting the superior crystal quality of ZnO on O₂ plasma activated MWCNTs.³¹ Consequently, Raman characterization results also validate the hypothesis that surface activation of the MWCNTs is essential for effective functionalization, i.e., stronger nucleation and binding of the MONCs onto the MWCNT surfaces.

The G peak represents the movement in the opposite direction of two neighboring carbon atoms in a graphitic sheet, hence indicating the presence of crystalline graphitic carbon in MWCNTs,¹⁰ while the D peak represents the defects in the curved graphite sheet, *sp*³ carbon, or other impurities.³³ The I_D/I_G ratio, where *I* corresponds to the peak area of the Lorentzian functions, is an estimate of the relative structural defects. Our preliminary characterization suggests that due to O₂ plasma activation, the relative intensity of the D-peak with respect to the G-peak (I_D/I_G ratio) of the MWCNT increases 13.5%. The results are presented in the supplementary material.⁴⁹ The probable reason for the increase in the intensity of the D-peak with respect to the G peak is the presence of reactive sites on the surface of the MWCNTs created by O₂. These sites are supposed to

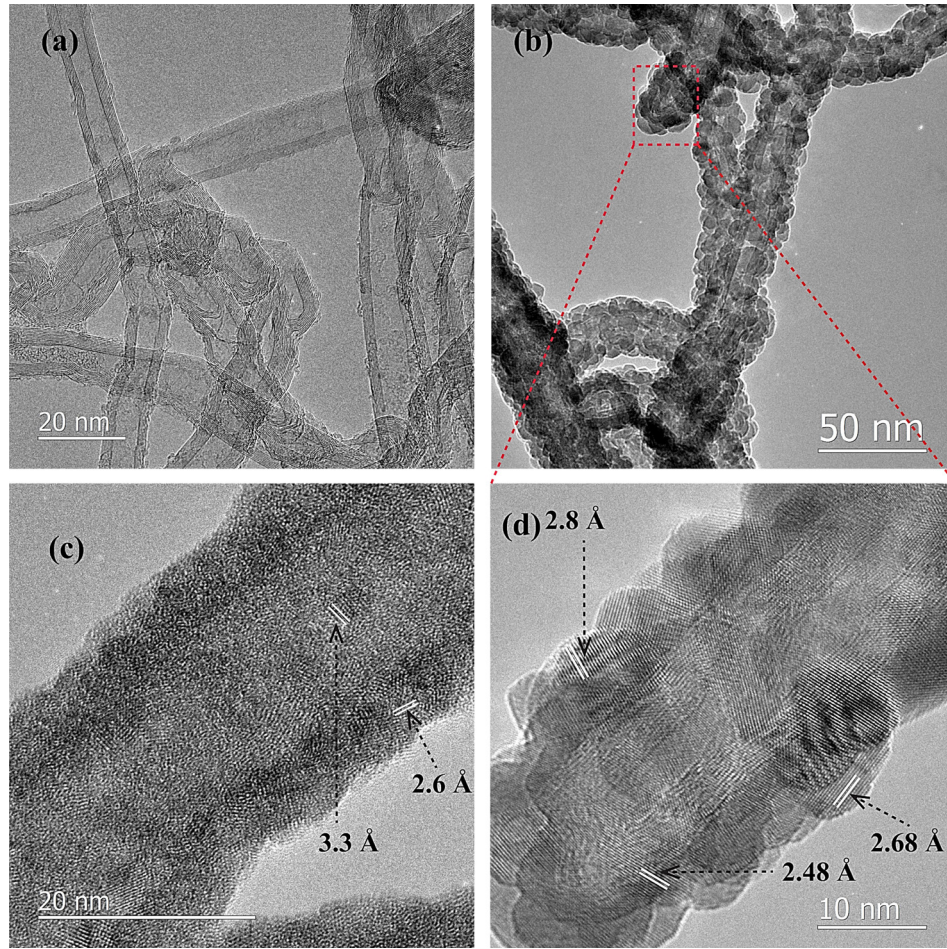


FIG. 3. (Color online) (a) TEM image of untreated but ZnO deposited MWCNTs. ZnO nanocrystals were not visible on the surface of these untreated MWCNTs. (b) Uniform distribution of atomic layer deposited ZnO nanocrystals on the UVO activated MWCNT surface. (c) High resolution TEM image of a SnO₂-MWCNT (ALD at 175 °C) sample showing interplanar spacings of 2.6 and 3.3 Å corresponding to $\langle 101 \rangle$ and $\langle 110 \rangle$ planes of SnO₂. (d) High resolution TEM image of a ZnO-MWCNT (ALD at 175 °C) sample showing interplanar spacings of 2.8, 2.68, and 2.48 Å corresponding to $\langle 100 \rangle$, $\langle 002 \rangle$, and $\langle 101 \rangle$ planes of ZnO.

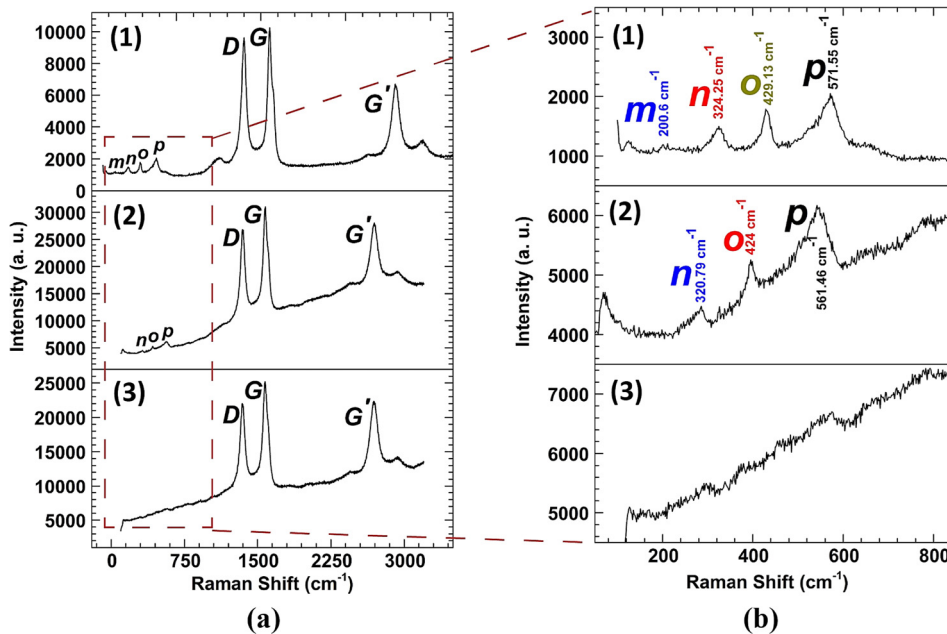


FIG. 4. (Color online) (a) Raman spectra obtained from the O₂ plasma activated ZnO functionalized MWCNT (top panel), UVO activated ZnO functionalized MWCNT (middle panel), and untreated but ZnO functionalized MWCNT (bottom panel). (b) Enlarged ZnO peaks in the range of 100–850 cm⁻¹ frequency shift.

enhance the uniform distribution of the metal oxide nanoparticles on the MWCNT surface.

B. Methane sensing

Our hypothesis is that MONCs facilitate chemisorption of methane gas molecules on the surface of the activated MWCNTs. We found that the resistance of the MONC-MWCNT sensors increases in the presence of a mixture of methane in dry air. The relative resistance change has been defined as

$$\Delta R/R = (R_{\text{methane}} - R_{\text{air}})/R_{\text{air}}.$$

A series of experiments were conducted to evaluate the effect of UVO and O₂ plasma treatments on the performance of the MONC-MWCNT sensor. To decouple the sensor response to CH₄ from the interference of variable RH, the RH inside the test chamber was kept constant and monitored in real time during each test period. The relative resistance of the sensor monotonically increased at room temperature when 10 ppm CH₄ in air was introduced to the test chamber. While maintaining a constant flow rate, when the incoming gas was switched from CH₄ to N₂, the relative resistance of the sensor decreased and returned to the baseline [Figs. 5(a)–5(c)]. The sensing mechanism could be elucidated from this phenomenon: the monotonic increase in the sensor's relative resistance is a result of absorption of CH₄ molecules on the MONC functionalized MWCNT surface.

Figure 5 also corroborates the assumption that surface activation is essential for effective functionalization of the MWCNT by MONCs and for the sensor to act reversibly in the presence and absence of 10 ppm CH₄ in air. Figures 5(a) and 5(b) show reproducible changes in the relative resistance of the surface activated ZnO-MWCNT sensor during alternating exposure to CH₄ and N₂. Figure 5(c) illustrates a

surface activated SnO₂-MWCNT chemoresistor sensor alternatively exposed to CH₄ and N₂ showing similarity to the ZnO-MWCNT results. No discernible signals were observed in the untreated (but ZnO NC deposited) MWCNT sensor [Fig. 5(d)].

At room temperature, the average relative resistance change $[\Delta R/R = (R_{\text{methane}} - R_{\text{air}})/R_{\text{air}}]$ was found to be $1.91 \pm 0.98\%$ for UVO activated and $10.5 \pm 1.01\%$ for O₂ plasma activated ZnO-MWCNT sensors. The results show that the O₂ plasma activation significantly enhances the affinity of the MONCs (in this case ZnO NCs) to the MWCNT surface in comparison to UVO activation. This enhanced affinity causes stronger electron transport through the ZnO-MWCNT junction, i.e., a larger resistance change in the presence of CH₄ at room temperature [Figs. 5(a) and 5(b)]. This is likely due to the better crystal quality of the ZnO NCs on O₂ plasma activated MWCNTs compared to UVO activated MWCNTs (as also observed from the Raman results in Fig. 4).

A novel UV-based recovery technique was recently presented by our group.³⁴ The sensor was first exposed to 10 ppm CH₄ in air for 30 min, and without interrupting the flow of CH₄, the sensor was irradiated with UV light until the sensor returned to its baseline resistance. No N₂ flow was used during the recovery. A recovery time of about 3 min was observed. The improvement in the recovery time, we believe, was due to the UV induced reduction of the desorption energy barrier of the CH₄ molecules at the sensor surface.⁵

To verify the sensor response to methane, the ZnO-MWCNT sensor was tested at varying CH₄ concentrations (2, 5, and 10 ppm in dry air) at room temperature. Methane of 2 and 5 ppm was obtained from the dilution of 10 ppm methane in synthetic air. The sensors were exposed to CH₄ for 10 min (gas phase) and then to nitrogen for 10 min

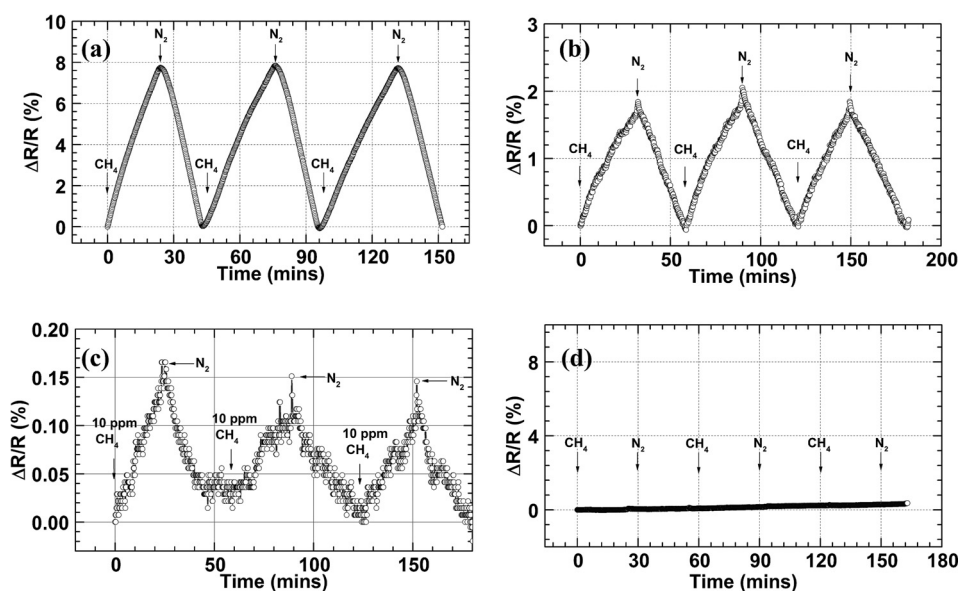


FIG. 5. Comparison of the dynamic sensor response $[\Delta R/R = (R_{\text{methane}} - R_{\text{air}})/R_{\text{air}}]$ of MONC-MWCNT sensors to 10 ppm CH₄ in dry air, followed by flushing with N₂ for sensor recovery. Each section of the figure shows $\Delta R/R$ for: (a) O₂ plasma treated ZnO functionalized, (b) a UVO treated ZnO functionalized, (c) a UVO treated SnO₂ functionalized, and (d) an untreated but ZnO deposited MWCNT sensor.

(desorbing phase), repeating this protocol in the entire set of experiments. The response from a representative sensor is shown in Fig. 6. The sensors were also tested and displayed zero cross-sensitivity to O₂. The cross-sensitivity to O₂ was determined to be insignificant comparing the sensitivity of the sensor with a variable dilution of O₂ in N₂, i.e., synthetic air (results not shown here).

The sensitivity of a semiconducting oxide gas sensor is defined as follows:^{5,6}

(1) for reducing gas

$$\Delta R/R = (R_{\text{gas}} - R_{\text{air}})/R_{\text{air}},$$

(2) for oxidizing gas

$$\Delta R/R = (R_{\text{air}} - R_{\text{gas}})/R_{\text{gas}},$$

where R_{air} is the resistance of the sensor in air and R_{gas} is the resistance of the sensor in the presence of gas and air.

We found that the resistance of the MONC-MWCNT sensors changes in the presence of a mixture of methane in air. The change in resistance is in accordance with the change in resistance of the SnO₂-MWCNT nanohybrid reported by Lu *et al.*,⁶ where they show that the resistance of the SnO₂-MWCNT nanohybrid decreases in the presence of oxidizing NO₂. A possible sensing mechanism has been reported by Lu *et al.*⁶ Target molecules, in this case NO₂, get directly adsorbed onto the SnO₂-MWCNT surface, facilitate electron transfer, and change the electrical conductivity of the hybrid nanostructure.

One can find references that describe the electronic properties of MWCNTs as metallic^{35,36} or semiconductive.^{6,37–39} However, ZnO and SnO₂ are widely known as n-type materials,^{6,32} and the presence of a reducing gas, such as CH₄, alters their charge concentration, resulting in a change in the resistance of the MONC-MWCNT conglomerate, which was observed experimentally.

A deeper investigation on the methane-functionalized CNT surface interaction is in order; however, this is beyond the scope of this paper. Furthermore, we are currently conducting experiments to study the electronic properties of surface pretreated metal oxide nanocrystal functionalized

MWCNTs, which will help us to understand their methane gas sensing mechanism more thoroughly.

Understanding the effect of RH is important in estimating the outdoor performance of microfabricated gas sensors. To examine the effect of RH on sensor performance, the change in the baseline relative resistance of the surface activated ZnO-MWCNT sensors was measured at room temperature due to a change in RH. Humidity was provided by a controlled flow of moist air (flow rate: 0.94 l/min) into a plastic test chamber (residence time: 4.5 min). The baseline relative resistance of the sensor increased by about 4% as the RH was increased from 10% to 91% and returned back to the original baseline once the RH was reduced back to 10%. This suggests a strong electron transfer between the MONC functionalized MWCNTs and water molecules (Fig. 7). Our ongoing research involves fabricating a network of MWCNTs selectively functionalized with various metal oxide nanoparticles with different sets of sensitivities to CH₄ and H₂O. By deconvoluting the constructive/destructive interference at various RH levels, the RH contribution can be effectively determined and separated from the device's response to CH₄.

We explored the relative resistance change for 10 ppm methane at two different RH levels.²⁶ While exposing the SnO₂-MWCNT sensor to 10 ppm of CH₄ in dry air at the higher RH (approximately 70%), a monotonic resistance increment was observed which was similar to the low RH tests where RH was held constant at 5%, as seen in Fig. 8. The sensor also equilibrated to its original response in a similar fashion when the chamber was purged with N₂. The response to CH₄ and signal-to-noise ratio reduced in comparison to those at lower RH, which we believe was a result of adsorbed H₂O molecules on the SnO₂-MWCNT sensor. Although the sensor showed a reduced response, it was still capable of detecting 10 ppm CH₄ in air at 70% RH. We observed a monotonic increase in the sensor resistance, while it was exposed to CH₄ at low and high RH, as well as a monotonic decrease (return to baseline) when CH₄ was purged with N₂ (Fig. 8). The sensor behavior is similar at both low and high humidities although the sensitivity is reduced at high RH. This is likely the result of absorbed H₂O molecules on the sensor surface. Water molecules are found to behave as electron donors on the surface of carbon

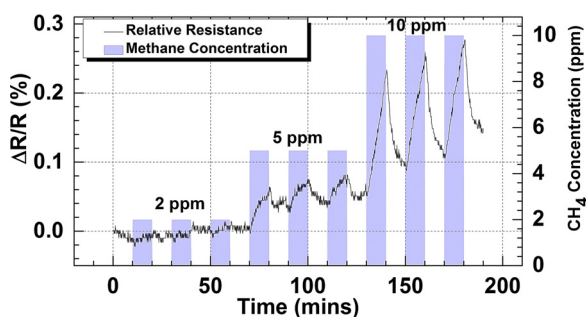


Fig. 6. (Color online) Relative resistance change of an O₂ plasma activated ZnO functionalized MWCNT sensor under exposure to 2, 5, and 10 ppm of CH₄ in the dry air mixture at room temperature. RH was kept constant at 2% during the experiment. A different metal electrode/CNT configuration was used, resulting in a smaller relative resistance change compared to Fig. 5(a).

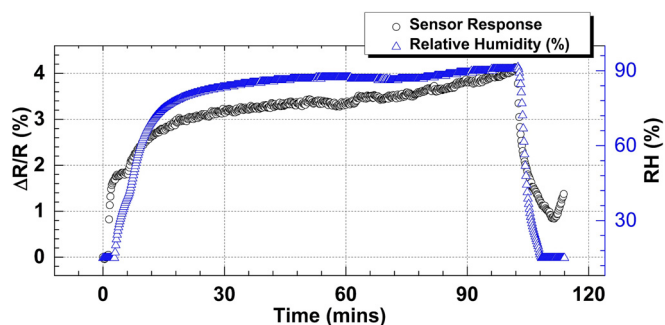


Fig. 7. (Color online) Relative resistance change [$\Delta R/R = (R_{\text{RH}} - R_{\text{air}})/R_{\text{air}}$] of the ZnO-MWCNT sensor, while the relative humidity inside the chamber was varied by a controlled flow of moist air. The right hand y-axis represents the RH inside the chamber during the test.

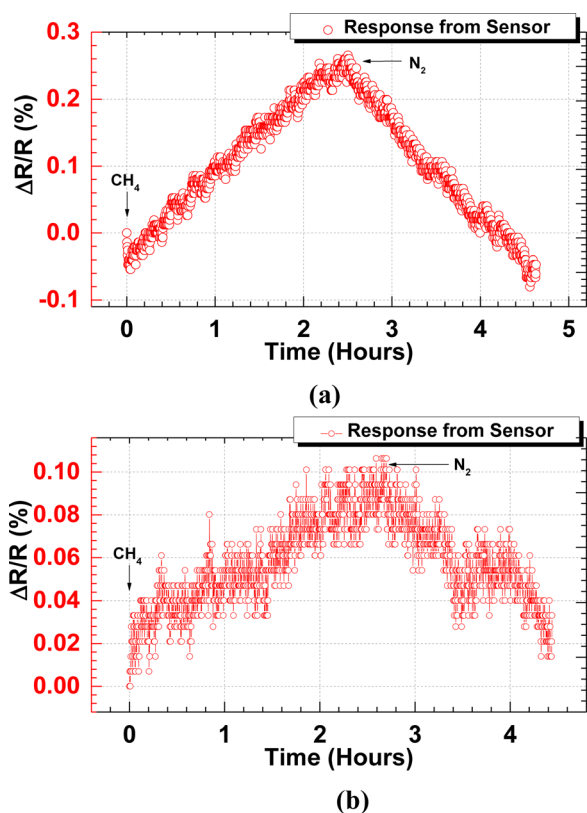


Fig. 8. (Color online) Relative resistance change of the SnO₂-MWCNT chemoresistor sensor while exposed to 10 ppm of CH₄ in dry air at (a) a lower RH (5%) and (b) a higher RH (70%) and was recovered by N₂. The circle symbol plot represents the relative resistance change [$\Delta R/R = (R_{RH} - R_{air})/R_{air}$] of the chemoresistor sensor (left hand, y-axis), while the triangle symbol plot represents the RH inside the test chamber recorded by a commercial RH data logger (right hand, y-axis). Reproduced with permission from Humayun *et al.*, *J. Vac. Sci. Technol.*, A **34**, 01A131 (2016) (Ref. 26).

nanotubes.^{40–42} It was reported that a hydrogen-bonded water monolayer forms around the nanotube at a fully water covered condition.⁴⁰ Na *et al.*⁴⁰ presented the change in electrical resistance as a function of relative humidity, which agrees with the result presented in Fig. 8, i.e., a decrease in the relative change in resistance (ΔR) at a high RH condition. This can be attributed to electron donation by the H₂O molecules on the sensor surface.^{40,42} Our ongoing work focuses on studying the response of the MONC-MWCNT sensor at a fixed ppm methane for multiple RH%.

The CH₄ sensor described here uses MWCNTs functionalized by MONCs to sense methane. We used two well known MONCs, ZnO and SnO₂, that are widely used

methane sensing materials and are inexpensive. ZnO and SnO₂ promote energetically favorable electron transport at the MO-MWCNT junction.^{6,20} The work function of ZnO was reported to be almost 4.64 (Ref. 43) or 5.2 eV,⁴⁴ while SnO₂ has a work function of 4.7 eV.⁶ The work functions of these MONCs are almost equal to the work function of MWCNTs (4.7–4.9 eV).^{6,45} Therefore, the Schottky barrier height at the MONC-MWCNT junction is low, facilitating electron transfer between MWCNTs and MONCs. The low Schottky barrier improves the overall sensitivity of the sensor (i.e., high $\Delta R/R$ at low ppm), making the hybrid MONC-MWCNT system a potentially superior sensing element to either of its constituent components.⁶

Table II compares the performance of our sensor with other published CNT CH₄ sensors. Note that although the sensor presented in Ref. 46 shows an equivalent performance to our sensors, it used wet chemically treated single walled carbon nanotubes (SWCNTs). Wet chemical treatment may be undesirable in CNT sensor fabrication as it is well known that acid treatments used in wet chemistry can considerably reduce the mechanical and electric performance of the tubes by introducing large numbers of defects,²¹ which might limit its reproducibility and reliability, as well as increase the cost of the sensor. Wet chemistry also involves additional steps, such as dissolution, sonication, mixing, and drying, which often causes undesirable agglomeration of treated CNTs.

IV. CONCLUSION

In summary, O₂ plasma activation has a stronger impact than UVO activation on enhancing the MONC functionalization of MWCNTs and thus on the response of the chemoresistive sensors to 10 ppm CH₄ in air. The strong relative resistance change in the presence of 10 ppm of CH₄ at room temperature is a consequence of: (1) strong electron transfer to the MONCs from CH₄ molecules, (2) energetically favorable electron transport at the MONC-MWCNT junction, and (3) enhanced affinity of the dry surface activated MWCNT to MONCs as a result of formation of active chemical groups. The O₂ plasma and UVO-based activation processes give rise to COOH, C=O, and C-OH functional groups on the MWCNT surface and hence enhance the nucleation and bonding of MONCs with the MWCNT. These treatments produce a strong reversible relative resistance change in the chemoresistors under iterative exposure to 10 ppm CH₄ in air and a relatively reduced response to lower concentrations. The response varies with RH, with a lower response at

TABLE II. Comparison of CNT chemoresistor sensors.

Material	Lowest detection limit	Operating temperature	Interference gases
Pd-SWCNT (Ref. 5)	15 ppm	Room temperature (RT)	Not mentioned (NM)
Pd-MWCNT (Ref. 14)	3 vol. %	RT	H ₂ , NH ₃
Pd-MWCNT (Ref. 11)	2 vol. %	RT	NM
Carbon nanofiber (Ref. 47)	500 ppm	RT	NM
Pt-CNT, Ru-CNT, Ag-CNT (Ref. 48)	0.7 vol. %	150 °C	CO ₂ , CO, NO ₂ , NH ₃
SWCNT (wet chemical treated) (Ref. 46)	2 ppm	RT	CO, SO ₂ , NH ₃
ZnO-MWCNT and SnO ₂ -MWCNT (This work)	2 ppm	RT	H ₂ O

higher RH as well as a lower detection limit. At low RH, the detection limit is between 2 and 5 ppm.

ACKNOWLEDGMENTS

The work performed at the Center for Nanoscale Materials and the Advanced Photon Source, Office of Science user facilities was supported by the U.S. Department of Energy, Office of Science, Office of Basic Energy Sciences, under Contract No. DE-AC02-06CH11357. The U.S. Environmental Protection Agency, through its Office of Research and Development, collaborated in the research described here. It has been subjected to Agency review and approved for publication. The authors would like to thank Scienta Omicron for loan of the Argus electron energy analyzer.

- ¹⁴“Overview of greenhouse gases,” last accessed: September 2, 2015, <http://epa.gov/climatechange/ghgemissions/gases/ch4.html>.
- ²D. Barreca, D. Bekermann, E. Comini, A. Devi, R. A. Fischer, A. Gasparotto, C. Maccato, G. Sberveglieri, and E. Tondello, *Sens. Actuator, B* **149**, 1 (2010).
- ³P. Fau, M. Sauvan, S. Trautweiler, C. Nayral, L. Erades, A. Maisonnat, and B. Chaudret, *Sens. Actuator, B* **78**, 83 (2001).
- ⁴T. Waitz, T. Wagner, T. Sauerwald, C.-D. Kohl, and M. Tiemann, *Adv. Funct. Mater.* **19**, 653 (2009).
- ⁵Y. Lu, J. Li, J. Han, H.-T. Ng, C. Binder, C. Partridge, and M. Meyyappan, *Chem. Phys. Lett.* **391**, 344 (2004).
- ⁶G. Lu, L. E. Ocola, and J. Chen, *Adv. Mater.* **21**, 2487 (2009).
- ⁷P. Qi, O. Vermesh, M. Grecu, A. Javey, Q. Wang, H. Dai, S. Peng, and K. Cho, *Nano Lett.* **3**, 347 (2003).
- ⁸C. Staii, A. T. Johnson, M. Chen, and A. Gelperin, *Nano Lett.* **5**, 1774 (2005).
- ⁹A. Felten, C. Bittencourt, J.-J. Pireaux, G. V. Lier, and J.-C. Charlier, *J. Appl. Phys.* **98**, 074308 (2005).
- ¹⁰Z. N. Utegulov, D. B. Mast, P. He, D. Shi, and R. F. Gilland, *J. Appl. Phys.* **97**, 104324 (2005).
- ¹¹D.-Q. Yang and E. Sacher, *J. Phys. Chem. C* **112**, 4075 (2008).
- ¹²E. H. Espinosa, R. Ionescu, C. Bittencourt, A. Felten, R. Erni, G. Van Tendeloo, J.-J. Pireaux, and E. Llobet, *Thin Solid Films* **515**, 8322 (2007).
- ¹³P. Kar and A. Choudhury, *Sens. Actuators, B* **183**, 25 (2013).
- ¹⁴Z. Li, J. Li, X. Wu, S. Shuang, C. Dong, and M. M. F. Choi, *Sens. Actuator, B* **139**, 453 (2009).
- ¹⁵Y. Li, H. Wang, Y. Chen, and M. Yang, *Sens. Actuator, B* **132**, 155 (2008).
- ¹⁶K. E. Aasmundtveit, B. Q. Ta, A. V. Ngo, O. Nilsen, and N. Hoivik, *2014 IEEE 14th International Conference on Nanotechnology (IEEE-NANO)*, Toronto, ON, Canada (IEEE, 2014).
- ¹⁷S. Boukhalfa, K. Evanoff, and G. Yushin, *Energy Environ. Sci.* **5**, 6872 (2012).

- ¹⁸M.-G. Willinger, G. Neri, E. Rauwel, A. Bonavita, G. Micali, and N. Pinna, *Nano Lett.* **8**, 4201 (2008).
- ¹⁹S. Heinze, J. Tersoff, R. Martel, V. Derycke, J. Appenzeller, and P. Avouris, *Phys. Rev. Lett.* **89**, 106801 (2002).
- ²⁰H. Zhang, N. Du, B. Chen, D. Li, and D. Yang, *Sci. Adv. Mater.* **1**, 13 (2009).
- ²¹A. Zamudio *et al.*, *Small* **2**, 346 (2006).
- ²²E. Najafi, J.-Y. Kim, S.-H. Han, and K. Shin, *Colloid Surf. A* **284**, 373 (2006).
- ²³C. Chen, B. Liang, A. Ogino, X. Wang, and M. Nagatsu, *J. Phys. Chem. C* **113**, 7659 (2009).
- ²⁴R. Larciprete, S. Gardonio, L. Petaccia, and S. Lizzit, *Carbon* **47**, 2579 (2009).
- ²⁵M. T. Humayun, R. Divan, L. Stan, A. Gupta, D. Rosenmann, L. Gundel, P. A. Solomon, and I. Paprotny, *J. Vac. Sci. Technol., B* **33**, 06FF01 (2015).
- ²⁶M. T. Humayun, R. Divan, Y. Liu, L. Gundel, P. A. Solomon, and I. Paprotny, *J. Vac. Sci. Technol., A* **34**, 01A131 (2016).
- ²⁷A. Ganguly, S. Sharma, P. Papakonstantinou, and J. Hamilton, *J. Phys. Chem. C* **115**, 17009 (2011).
- ²⁸P.-L. Girard-Lauriault, R. Illgen, J.-C. Ruiz, M. R. Wertheimer, and W. E. S. Unger, *Appl. Surf. Sci.* **258**, 8448 (2012).
- ²⁹U. Zielke, K. J. Hüttinger, and W. P. Hoffman, *Carbon* **34**, 983 (1996).
- ³⁰P. Bindu and S. Thomas, *J. Theor. Appl. Phys.* **8**, 123 (2014).
- ³¹R. Cuscó, E. Alarcón-Lladó, J. Ibanez, L. Artús, J. Jiménez, B. Wang, and M. J. Callahan, *Phys. Rev. B* **75**, 165202 (2007).
- ³²X. Li, C. Li, Y. Zhang, D. P. Chu, W. I. Milne, and H. J. Fan, *Nano Res. Lett.* **5**, 1836 (2010).
- ³³E. F. Antunes, A. O. Lobo, E. J. Corat, and V. J. Trava-Airoldi, *Carbon* **45**, 913 (2007).
- ³⁴M. T. Humayun, R. Divan, L. Stan, D. Rosenmann, D. Gosztola, L. Gundel, P. A. Solomon, and I. Paprotny, *IEEE Sens. J.* **16**, 8692 (2016).
- ³⁵R. V. Gelamo, F. P. Rouxinol, C. Verissimo, A. R. Vaz, M. A. Bica de Moraes, and S. A. Moshkalev, *Chem. Phys. Lett.* **482**, 302 (2009).
- ³⁶W.-S. Cho, S.-I. Moon, Y.-D. Lee, Y.-H. Lee, J.-H. Park, and B. K. Ju, *IEEE Electron Device Lett.* **26**, 498 (2005).
- ³⁷J. Zhang, X. Liu, G. Neri, and N. Pinna, *Adv. Mater.* **28**, 795 (2016).
- ³⁸H. Dai, *Acc. Chem. Res.* **35**, 1035 (2002).
- ³⁹O. K. Varghese, P. D. Kichambre, D. Gong, K. G. Ong, E. C. Dickey, and C. A. Grimes, *Sens. Actuator, B* **81**, 32 (2001).
- ⁴⁰P. S. Na *et al.*, *Appl. Phys. Lett.* **87**, 093101 (2005).
- ⁴¹K. G. Ong, K. Zeng, and C. A. Grimes, *IEEE Sens. J.* **2**, 82 (2002).
- ⁴²J.-W. Han, B. Kim, J. Li, and M. Meyyappan, *J. Phys. Chem. C* **116**, 22094 (2012).
- ⁴³H. Moormann, D. Kohl, and G. Heiland, *Surf. Sci.* **80**, 261 (1979).
- ⁴⁴X. Bai, E. G. Wang, P. Gao, and Z. L. Wang, *Nano Lett.* **3**, 1147 (2003).
- ⁴⁵M. Shiraishi and M. Ata, *Carbon* **39**, 1913 (2001).
- ⁴⁶A. Hannon, Y. Lu, J. Li, and M. Meyyappan, *Sensors* **16**, 1163 (2016).
- ⁴⁷R. K. Roy, M. P. Chowdhury, and A. K. Pal, *Vacuum* **77**, 223 (2005).
- ⁴⁸M. Penza, R. Rossi, M. Alvisi, and E. Serra, *Nanotechnology* **21**, 105501 (2010).
- ⁴⁹See supplementary material at <http://dx.doi.org/10.1116/1.4993579> for the Raman results.